Experimental validation of a two equation RANS transitional turbulence model for compressible microflows

Published Version:
Rehman D., Morini G.L. (2020). Experimental validation of a two equation RANS transitional turbulence model for compressible microflows. INTERNATIONAL JOURNAL OF HEAT AND FLUID FLOW, 86, 1-11 [10.1016/j.ijheatfluidflow.2020.108711].

Availability:
This version is available at: https://hdl.handle.net/11585/776679 since: 2020-10-29

Published:
DOI: http://doi.org/10.1016/j.ijheatfluidflow.2020.108711

(Article begins on next page)

Danish Rehman, Gian Luca Morini,

Experimental validation of a two equation RANS transitional turbulence model for compressible microflows

International Journal of Heat and Fluid Flow,Volume 86, 2020, 108711

Experimental Validation of a Two Equation RANS Transitional Turbulence Model for Compressible Microflows

Danish Rehman[a], Gian Luca Morini[a]

[a] *Microfluidics Laboratory, Dept. of Industrial Eng. Via del Lazzaretto 15/5, University of Bologna, Bologna 41031, Italy*

Abstract

Laminar-to-turbulent flow transition in microchannels can be useful to enhance mixing and heat transfer in microsystems. Typically, the small characteristic dimensions of these devices hinder in attaining higher Reynolds numbers to limit the total pressure drop. This is true especially in the presence of a liquid as a working medium. On the contrary, due to lower density, Reynolds number larger than 2000 can be easily reached for gas microflows with an acceptable pressure drop. Since microchannels are used as elementary building blocks of micro heat exchangers and micro heat-sinks, it is essential to predict under which conditions, the laminar-to-turbulent flow transition inside such geometries can be expected. In this paper, experimental validation of a two equations transitional turbulence model, capable of predicting the laminar-to-turbulent flow transition for internal flows as proposed by Abraham et al. (2008), is presented for the first time for microchannels. This is done by employing microchannels in which Nitrogen gas is used as a working fluid. Two different cross-sections namely circular and rectangular are utilized for numerical and experimental investigations. The inlet mass flow rate of the gas is varied to cover all the flow regimes from laminar to fully turbulent flow. Pressure loss experiments are performed for both cross-sectional geometries and friction factor results from experiments and numerical simulations are compared. From the analysis of the friction factor as a function of the Reynolds number, the critical value of the Reynolds number linked to the laminar-to-turbulent transition has been deter-

Preprint submitted to Heat and Fluid Flow *September 12, 2020*

mined. The experimental and numerical critical Reynolds number for all the tested microchannels showed a maximum deviation of less than 12%. These results demonstrate that the transitional turbulence model proposed by Abraham et al. (2008) for internal flows can be extended to microchannels and proficiently employed for the design of micro heat exchangers in presence of gas flows.

Keywords: compressibility, laminar-to-turbulent flow transition, friction factor, micro heat exchangers

---

1. Introduction

The prediction of the laminar-to-turbulent transition in microtubes (MTs) and microchannels (MCs) is very important for the design of microdevices in which internal flows are present such as heat sinks and micro heat exchangers. After the pioneering work of Tuckerman and Pease (1981), most of the earlier experimental groups involved in the analysis of internal flows within microchannels reported an anticipated laminar-to-turbulent flow transition in MCs like Peiyi and Little (1983), Choi et al. (1991), Peng et al. (1994) among others. Whereas, a few groups like Harms et al. (1999), Adams et al. (1999) confirmed the agreement to the typical rules of the laminar-to-turbulent transition in conventional tubes. Recent reviews like those of Asadi et al. (2014), Dixit and Ghosh (2015) conclude that experimental data obtained in the recent decade seems to confirm that single-phase flows in MCs follow conventional laws. A comprehensive review outlining possible reasons for deviations from macro theory in earlier reported experiments is due to Morini (2004b), according to which macro theory holds for MC flows as long as scaling effects can be considered negligible. Morini (2004b) individuated the main scaling effects (compressibility, rarefaction, viscous dissipation, electro osmotic effects, and surface roughness) that need to be verified before interpreting experimental results which can be responsible for deviation from conventional correlations. In another work, Morini (2004a) gathered previously published experimental data for laminar-to-turbulent flow transition in MCs and compared them with macro laws. The analysis in rectangular microchannels showed that various published results for critical Reynolds number (Re_c) can be explained by using the Obot-Jones model developed for conventional channels with a cross-section different from circular (which is the case of large part of microchannels). In fact, Obot (1988) demonstrated that the critical Reynolds number linked to the laminar-to-turbulent transition is a function of the cross-sectional geometry of the channel.

Laminar-to-turbulent flow transition even in conventional sized channels is still an open field of investigation. Based on original experiments of Reynolds (1883), the transition in pipe flow occurs when the Reynolds number reaches a critical value (Re_c) close to 2000 in the presence of a tube with a rough entrance. The full comprehension of the physical processes, which trigger such flow transition when the flow rate is increased, is yet to be achieved. Thus, research investigation in this domain is very active using sophisticated experimental and theoretical approaches, as evidenced by the works of Barkley et al. (2010), Avila et al. (2011), Barkley et al. (2011). Pipe flow experiments of Avila et al. (2011) showed that when the flow velocity is such that Re is lower than its critical value, turbulence was not sustained. Even if turbulent puffs were generated in the flow field, they were decayed swiftly by the surrounding laminar flow when the Re was lower than its critical value. This process is referred to as relaminarization. Above $Re_c = 2040$, the splitting process of these turbulent puffs outweighed the decay and hence turbulence could sustain. Afterward, turbulent puffs increased their size and the whole flow field suddenly exhibited a disordered motion. Later, Barkley et al. (2011) performed experiments on 10 mm pipe and 5 mm square duct. They introduced the perturbations in the flow field at a precise location along the length to initiate the turbulence. They also conducted Direct Numerical Simulations (DNS) of the flow field and showed that even when the flow is fully turbulent, just by modifying the velocity profile to more plug shaped caused the fully turbulent flow to break into turbulent puffs that were experimentally observed for $Re < 2300$. Such DNS inspired experiments were then conducted by Kühnen et al. (2018) who demonstrated how sustained turbulence can be destabilized and flow relaminarized in the pipe. Similarly, flow visualization as well as pressure drop studies, have been utilized to determine Re_c for microflows (Li and Olsen (2006), Wibel and Ehrhard (2009), Kim (2016)).

Due to the large difference in terms of density between working fluid and seeding particles, optical experimental techniques like μPIV are not recommended for gas flows in MCs and therefore a pressure drop study (Moody chart) remains the only useful experimental tool to determine the critical value of the Reynolds number (Re_c). Such analysis for gas flows in 11 different microtubes with $D_h = 125 - 180\ \mu m$ has been presented by Morini et al. (2009). By comparing their results with previously published gas flow pressure drop studies, it was shown that if friction factor is calculated by taking into account compressibility effects and minor losses, Re_c was in between $1800 - 2000$, in complete disagreement with the earlier transitions reported by other groups like Peiyi and Little (1983), Kandlikar et al. (2005).

As highlighted earlier, aside from experimental and analytical observations, DNS has been applied to understand the physics of flow transition like in the case of Barkley et al. (2011), Wu et al. (2015), Kühnen et al. (2018). However, due to the lower computational cost, Reynolds-Averaged Navier Stokes equations (RANS) based turbulence modeling is still preferred in industrial environments for engineering design goals. A breakthrough in modeling transitional flow using two equations turbulence models is due to Menter et al. (2006). They augmented the original Shear Stress Transport (SST) $k-\omega$ model (Menter (1994)) to incorporate flow transition based upon two additional intermittency transport equations. This model was later modified to be implemented into commercial CFD codes (Menter and Langtry (2012)). Although originally developed for external flows, constants present in the Menter's model were modified by Abraham et al. (2008) to predict laminar-to-turbulent transition in internal flows. It was shown for pipe flow that the fine-tuned model predicted laminar and fully turbulent friction factors similar to that of Poiseuille's law and Blasius law respectively. Therefore, transitional behavior was deemed to be representative of reality. The modification proposed by Abraham et al. (2008) for the transitional turbulence model of Menter et al. (2006) has not been validated experimentally for internal flows nor for microchannels. Considering this, the current work aims to experimentally validate this transitional turbulence model for gas microflows using the modified form as proposed by Abraham et al. (2008). The experimental validation will be made by observing the variation of the values assumed by the friction factor as a function of the Reynolds number. Both semi-local and average values of friction factors will be used in this validation.

2. Experimental Setup and Data Reduction

Pressure loss experiments are performed for a commercial MT (Upchurch®) and two rectangular MCs fabricated by milling a PMMA plastic sheet using a micromilling machine (Roland® MDX-40A). Dimensions and inner surface roughness of MCs are measured using an optical profiler (Talysurf CCI). For MT, a value of the surface roughness similar to that of Morini (2004a), Morini et al. (2009), Yang (2012), was extracted from SEM imaging of the stainless steel MTs. The measured average width (w), height (h), aspect ratio ($\alpha = h/w$) and surface roughness (ε) of investigated channels are reported in Table 1. Experimental test bench and a schematic of MC assembly used in this work are

Table 1: Channels geometry used for experiments.

Channel	h (μm)	w (μm)	α	D_h (μm)	ε (μm)
MT	-	-	1	1016	1
MC1	250	360	0.694	295	1.05
MC2	134	554	0.241	215	0.9

shown in Figure 1. Pressurized Nitrogen gas is allowed to enter MC assembly perpendicular to the axial direction of MC and leaves perpendicularly as well through the outlet manifold. In the case where experiments are performed for circular cross section, MC assembly is simply replaced by attaching MT directly at the inlet of the test bench using a commercial reducer/manifold. The total pressure drop between the inlet and the outlet of the MC/MT assembly is measured by means of a differential pressure transducer (Validyne DP15) with an interchangeable sensing element that allows accurate measurements over the whole range of encountered pressures. Atmospheric pressure is measured using an absolute pressure sensor (Validyne AP42). To measure the temperature at the entrance of the MC/MT assembly a K-type, calibrated thermocouple is used. Thermocouple voltage and an amplified voltage of pressure sensors are fed to internal multiplexer board of Agilent 39470A which is used as a switch. Voltages from the switch are measured using Agilent 34420A with a $7-1/2$ digits resolution and are finally stored in a PC using a Labview® program.

Considering one dimensional flow of ideal gas, average Fanning friction factor between inlet '*in*' and outlet '*out*' of a MC/MT with length L can be obtained by using the following expression for a compressible flow as indicated by Kawashima and Asako (2014):

$$f_f = \frac{D_h}{L}\left[\frac{p_{in}^2 - p_{out}^2}{RT_{av}\dot{G}^2} - 2\ln\left(\frac{p_{in}}{p_{out}}\right) + 2\ln\left(\frac{T_{in}}{T_{out}}\right)\right] \tag{1}$$

where p and T denote cross sectional average pressure and temperature of the gas and the subscripts 'in' and 'out' represent the inlet and the outlet of MC/MT, respectively. T_{av} is the average temperature of the gas between inlet and outlet of MC/MT, and $\dot{G}$ is the mass flux ($\dot{G} = \frac{\dot{m}}{A}$). Hydraulic diameter of a rectangular MC is defined as:

$$D_h = \frac{2wh}{w+h} \tag{2}$$

Reynolds number at the inlet of MC/MT can then be calculated using measured mass flow rate and calculated viscosity at inlet temperature with the following equation:

$$Re = \frac{\dot{m}D_h}{\mu A} \tag{3}$$

In addition, under the hypothesis of adiabatic compressible flow, the energy balance for one dimensional Fanno flow, between inlet '*in*' and any other cross section at a distance '*x*' from the inlet of the MC/MT yields the following quadratic equation for the estimation of average cross-sectional temperature as

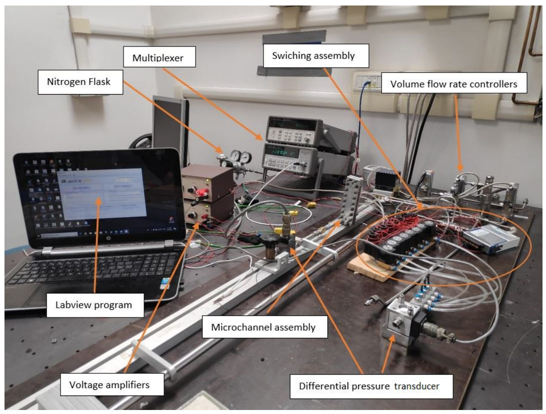

(a)

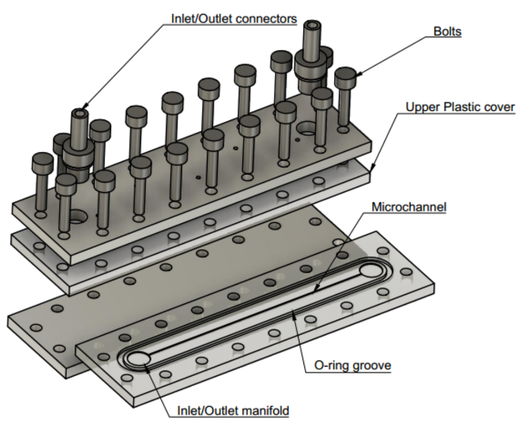

(b)

Figure 1: Experimental setup (**a**), and an exploded view of MC assembly (**b**).

demonstrated by Kawashima and Asako (2014):

$$\left(\frac{\rho_{in}^2 u_{in}^2 R^2}{2c_p p_x^2}\right) T_x^2 + T_x - \left(T_{in} + \frac{u_{in}^2}{2c_p}\right) = 0 \tag{4}$$

Finally, knowing the average pressure and temperature in a specific cross-section, average density and velocity of compressible gas can be obtained using the ideal gas law (Eq. 8) and continuity equations, respectively. An initial estimate of the gas velocity at MC/MT inlet is made using the measured mass flow rate and density of the gas at the inlet manifold entrance. MC/MT inlet properties are then calculated by assuming an isentropic expansion between the inlet of the assembly and the MC/MT. For further details on the equations that are solved iteratively to determine the inlet flow properties, the reader is referred to the previous works (Rehman et al. (2019), Hong et al. (2016)). Once inlet conditions are determined, temperature at MC/MT outlet can be easily evaluated using Eq. 4 given the local pressure is known. In current work, a hypothesis of perfect expansion is considered which essentially assumes atmospheric pressure at the MC/MT outlet ($p_{out} = p_{atm}$). This assumption holds if the dynamic conditions of gas flow are far from choking (Rehman et al. (2019)). Utilizing the outlet temperature evaluated by Eq. 4 and under perfect expansion assumption, average Fanning friction factor of MC/MT can finally be calculated using Eq. 1.

In order to assess the accuracy of the experimental measurements, the uncertainty associated to each instrument used in the experimental campaigns is reported in Table 2. In a detailed study, Yang (2012), based on the theory of

Table 2: Typical uncertainties of instruments used.

Instrument	**Range (0–Full Scale (FS))**	**Uncertainty**
Volume flow rate controllers	0–5000 nmL/min	± 0.5% FS
Pressure sensors	0–22, 0–86 & 0–1460 kPa	± 0.25% FS
K-type thermocouple	0–100 °C	± 0.25% FS

error propagation, highlighted that uncertainty in the evaluation friction factor is highly influenced by the uncertainty on the hydraulic diameter. In the present case, the uncertainty on the hydraulic diameter, evaluated by using an optical profilometer to measure both height (h) and width (w) of the MC, is of the order of 1.5%. The uncertainty associated to the measurement of L is around 0.4%. Therefore, the uncertainty in evaluating f_f (with Eq. 1) and Re (with Eq. 3) is estimated to be equal to ±10% and ±3%, respectively. All these uncertainties are summarized in Table 3.

Table 3: Typical uncertainties of experimentally deduced parameters based on theory of propagation.

Calculated Parameter	**Uncertainty**
D_h	±5%
Re	±3%
f_f	±10%

3. Mathematical Model

Internal flow physics of a compressible gas is governed by the following conservation equations of mass, momentum and energy:

$$\frac{\partial \rho u_i}{\partial x_i} = 0, \tag{5}$$

$$\frac{\partial \rho u_i}{\partial t} + \frac{\partial}{\partial x_j}\rho(u_j u_i) = -\frac{\partial p}{\partial x_i} + (\mu + \mu_t)\,\frac{\partial^2 u_i}{\partial x_j \partial x_j}, \tag{6}$$

$$\rho C_\mu u_i \frac{\partial T}{\partial x_i} = -p\frac{\partial u_i}{\partial x_i} + \lambda \frac{\partial^2 T}{\partial {x_i}^2} - \tau_{ij}\frac{\partial u_j}{\partial x_i}, \tag{7}$$

where i,j=1,2,3 are used to indicate three spatial directions; u_i represents the Cartesian velocity components in longitudinal, lateral and normal directions respectively; p is the pressure; ρ is the fluid density; T is the average fluid cross sectional temperature, μ is the fluid dynamic viscosity and μ_t is turbulent viscosity. For a laminar compressible fluid flow, there are 6 unknowns (u, v, w, p, ρ, T) for aforementioned set of 5 equations from Eqs. (5)-(7). An additional constitutive law is therefore used to complete the solution procedure for the complete set of Navier Stokes (NS) equations, as follows:

$$p = \rho RT, \tag{8}$$

where R is the specific gas constant. In order to proceed for a steady state solution of turbulent Reynold average NS (RANS) equations, the closure problem has been addressed in the literature by various models such as $k-\epsilon$ (Launder and Spalding (1974)) and Wilcox $k-\omega$ (Wilcox (1988, 2008)), to name a few. In the current work a shear stress transport (SST) model presented by Menter (1994) is used. This model uses $k-\omega$ approximation close to the walls and switches to $k-\epsilon$ far from the wall. The closure problem is dealt with the following two transport equations for modelling turbulent kinetic energy (k) and specific rate of turbulent destruction (ω):

$$\frac{\partial(\rho u_i k)}{\partial x_i} = P_k - \beta_1 \rho k \omega + \frac{\partial\left(\left(\mu + \frac{\mu_t}{\sigma_k}\right)\frac{\partial k}{\partial x_i}\right)}{\partial x_i}, \tag{9}$$

$$\frac{\partial(\rho u_i \omega)}{\partial x_i} = \chi\rho S^2 - \beta_2 \rho k \omega^2 + \frac{\partial\left(\left(\mu + \frac{\mu_t}{\sigma_\omega}\right)\frac{\partial \omega}{\partial x_i}\right)}{\partial x_i} + 2(1-F_1)\rho\frac{1}{\sigma_{\omega 2}\omega}\frac{\partial k}{\partial x_i}\frac{\partial \omega}{\partial x_i}, \tag{10}$$

where P_k is the rate of kinetic energy production, σ_k and σ_ω are the equivalents of Prandtl number for the transport of turbulent kinetic energy and specific rate of turbulent destruction, respectively. Moreover subscripts 1 and 2 for these σ_k and σ_ω represent different constants assumed for original $k-\omega$ model close to the wall and $k-\epsilon$ far from the wall, respectively. S is the absolute value of shear strain rate and χ, β_1 & β_2 are SST model constants. F_1 is a blending function that allows to switch from standard $k-\epsilon$ model to $k-\omega$ in order to better simulate the low Reynolds number region.

For most industrial problems, laminar flows are solved by NS equations whereas turbulent flows are dealt with RANS equations as described above. In the transitional flow regime between laminar and turbulent, computationally expensive models such as Large Eddy Simulations (LES) and DNS are applied where the transient evolution of the turbulence scales is modelled in the computational domain. Although accurate in predictions of flow characteristics, computational cost associated to these modelling techniques is enormous as compared to RANS and therefore are limited to accurate scientific evaluations. The two equation transport model (RANS) due to Menter et al. (2006) is coupled to two additional transport equations for the evaluation of a so called intermittency factor (γ). Its role is to diminish turbulence production for flow conditions that are not fully turbulent and its value is between 0 and 1. Evaluation of γ however, depends on another local flow property, the momentum thickness Reynolds ($\tilde{R}e_{\theta t}$), which describes the local stability status of the flow in the near wall region. These two additional transport equations are the following:

$$\frac{\partial(\rho\gamma)}{\partial t} + \frac{\partial(\rho u_i \gamma)}{\partial x_i} = P_{\gamma 1} - E_{\gamma 1} + P_{\gamma 2} - E_{\gamma 2} + \frac{\partial\left(\left(\mu + \frac{\mu_t}{\sigma_f}\right)\frac{\partial\gamma}{\partial x_i}\right)}{\partial x_i} \tag{11}$$

$$\frac{\partial(\rho\tilde{R}e_{\theta t})}{\partial t} + \frac{\partial(\rho u_i \tilde{R}e_{\theta t})}{\partial x_i} = P_{\theta t} + \frac{\partial\left(\sigma_{\theta t}(\mu + \mu_t)\frac{\partial \tilde{R}e_{\theta t}}{\partial x_i}\right)}{\partial x_i} \tag{12}$$

A detailed explanation of all the terms of Eqs. (11) and (12) can be found in Menter et al. (2006), ANSYS (2018). Only the most relevant terms are presented here starting from the transition source in Eq. (11) for intermittency:

$$P_{\gamma 1} = F_{length}\rho S(\gamma F_{onset})^{c_{a1}} \tag{13}$$

$$E_{\gamma 1} = c_{e1} P_{\gamma 1}\gamma \tag{14}$$

where F_{onset} is used to trigger the intermittency γ production and its formulation is a function of vorticity Reynolds number $Re_\nu = \frac{\rho y^2 S}{\mu}$ ANSYS (2018). F_{length} is obtained from correlations and it is dependent on $\overline{Re}_{\theta t}$; the detail about the correlations proposed for these two terms can be found in Menter and Langtry (2012). In Eq. 11, the destruction/relaminarization sources are defined as follows:

$$P_{\gamma 2} = c_{a2}\rho\Omega\gamma F_{turb} \tag{15}$$

$$E_{\gamma 2} = c_{e2} P_{\gamma 2}\gamma \tag{16}$$

where Ω denotes the magnitude of the absolute vorticity rate, $F_{turb} = e^{-(\frac{R_t}{4})^4}$ and $R_t = \frac{\rho k}{\mu\omega}$. Another important term in Eq. 11 is the production of $\tilde{R}e_{\theta t}$, defined as follows:

$$P_{\theta t} = c_{\theta t}\frac{\rho}{t}(Re_{\theta t} - \tilde{R}e_{\theta t})(1 - F_{\theta t}) \tag{17}$$

where t is a time scale that is present for dimensional reason and $F_{\theta t}$ is a blending function that allows to turn off the source terms in the boundary layer where the scalar quantity $\tilde{R}e_{\theta t}$ is only diffusing.

Coupling between the intermittency equations and SST model can be done by multiplying γ to the kinetic energy production term P_k; a modified form of Eq. (9) can be written as:

$$\frac{\partial(\rho u_i k)}{\partial x_i} = \gamma P_k - \beta_1 \rho k\omega + \frac{\partial\left(\left(\mu + \frac{\mu_t}{\sigma_k}\right)\frac{\partial k}{\partial x_i}\right)}{\partial x_i}, \tag{18}$$

As mentioned, γ is calculated by coupling Eqs. (11) & (12). The solution of Eq. (18) & (10) gives the values of k and ω which can be then utilized to obtain the turbulent viscosity μ_t:

$$\mu_t = \frac{a\rho k}{max(a\omega, SF_2)} \tag{19}$$

where a is a constant and F_2 is another blending function that limits the value of turbulent viscosity inside the boundary layer.

The model of Menter et al. (2006) represents a great breakthrough in transition prediction because it was formulated taking into account only local variables which makes it compatible with modern CFD codes that are 3D and parallel. However, it is worth mentioning that all the model constants recalled in the Menter's model were based on a series of experimental results obtained for external flows. Hence in its original form, this SST transitional turbulence model is not suitable for modelling internal flows, although it has been applied to study the transient turbulent channel flow by Gorji et al. (2014). Model constants proposed originally in the Menter's $\gamma - Re_\theta$ SST transitional turbulence model, in order of appearance in eqs. (13) - (17), are:

$$c_{a1} = 0.5;\ c_{e1} = 1.0;\ c_{a2} = 0.03;\ c_{e2} = 50;\ \sigma_f = 1.0;$$
$$c_{\theta t} = 0.03;\ \sigma_{\theta t} = 10;$$

To extend the use of Menter's model to internal flows, Abraham et al. (2008) later modified the constants of the Eqs. (16) & (17) using an iterative method such that transition in pipe flows was in between a generally accepted range of $2300 < Re < 4000$. Coefficients which predicted the transition at a Re lower than 2300 were not considered. The intermittency coefficient c_{e2} was increased from 50.0 to 70.0, and $c_{\theta t}$ was decreased from 0.03 to 0.015. Authors showed that by simply changing two values of the original coefficients of the original Menter's transitional model (Menter et al. (2006)), transitional characteristics of pipe flows can be predicted. In the current work, similar values of these coefficients as proposed by Abraham et al. (2008), Minkowycz et al. (2009) have been used.

4. Numerical Implementation

For the implementation of the above explained mathematical model using γ-Re_θ transitional turbulence model, numerical replicas of the experimental channels (Table 1) were generated in ANSYS-CFX environment (ANSYS (2018)). Computational models of both cross sectional geometries and their respective meshing strategies are detailed in the following:

4.1. Microtube

Test section schematic representing a MT is shown in Figure 2. A commercial reducer is also modelled in the computational domain that connects the gas piping to the MT inlet. Due to axisymmetric nature of the gas flow in MT, only a slice ($\theta = 10^o$) is modelled as the computational domain with rotational periodicity boundary condition on the side walls. This allows to save considerable computational time by using a smaller number of mesh elements. Dimensions of the reducer are also shown in Figure 2b. Length (L) of the MT varies in different set of numerical simulation and experimental runs. However, dimensions of the reducer and hydraulic diameter (D_h) are the same for all cases. MT geometric model is designed in Workbench Design Modeler and is meshed

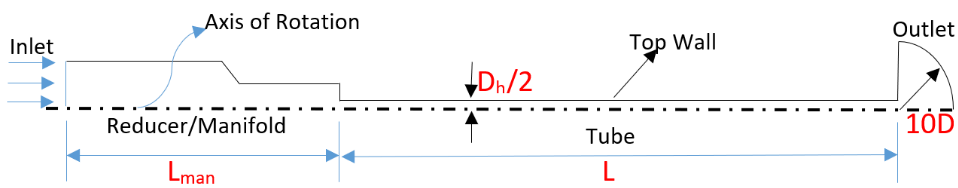

(a)

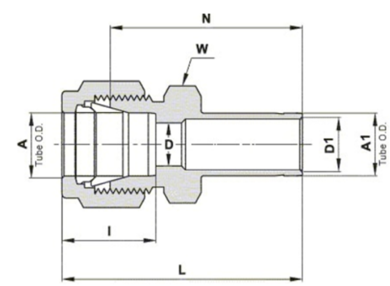

Label	Dimension (mm)	Label	Dimension (mm)
A	1.58	I	0.34
A1	6.35	N	27.68
D	1.27	L	31.5

(b)

Figure 2: Computational domain for MT cross section (**a**), reducer and associated dimensions (**b**).

using ANSYS meshing software. A structured mesh is generated for the MT as shown in Figure 3. Number of divisions along the radial direction (r) for the inlet reducer/manifold and outlet are set equal to radial divisions of the MT whereas 15 meshing nodes are used along the length of reducer and outlet.

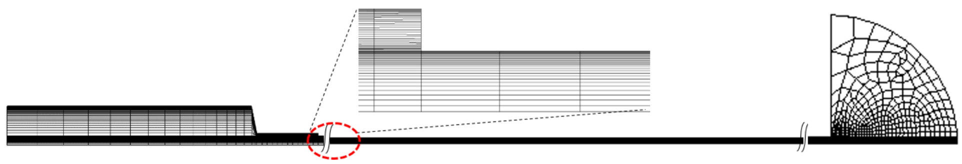

Figure 3: Mesh of the MT geometry.

4.2. Microchannel

To have a better understanding of the flow physics, symmetry boundary condition is not applied in the case of rectangular cross-section and therefore a complete 3D geometry as shown in Figure 4 is used as computational domain. The number of node points in the height direction of the MC is reduced accordingly if the height is reduced in the simulation model to maintain better element quality. A structured mesh locally refined at the walls of the MC and manifolds is employed. Orthogonality of mesh elements inside MC is between 0.95–1 in all the simulated cases. Reducers and manifolds are also simulated along with the MCs. Height of the reducer (H_{in}, see Figure 4) is 30 mm with an internal diameter of 4 mm. Whereas the diameter of the circular manifolds is 9 mm and height (H_{man}) is kept the same as the height of the simulated MC ($H_{man} = h$). Dimensions of these parts are chosen based upon the experimentally tested MC assembly. The outlet is perfectly symmetric to the inlet manifold and therefore two 90 degrees bends are present in the flow domain and may influence the total pressure drop and hence friction factor evaluation.

4.3. Solution Procedure

In order to obtain the desired Re, mass flow calculated using Eq. (3) is imposed at the inlet of MT/MC. Ideal nitrogen gas enters the reducer/manifold

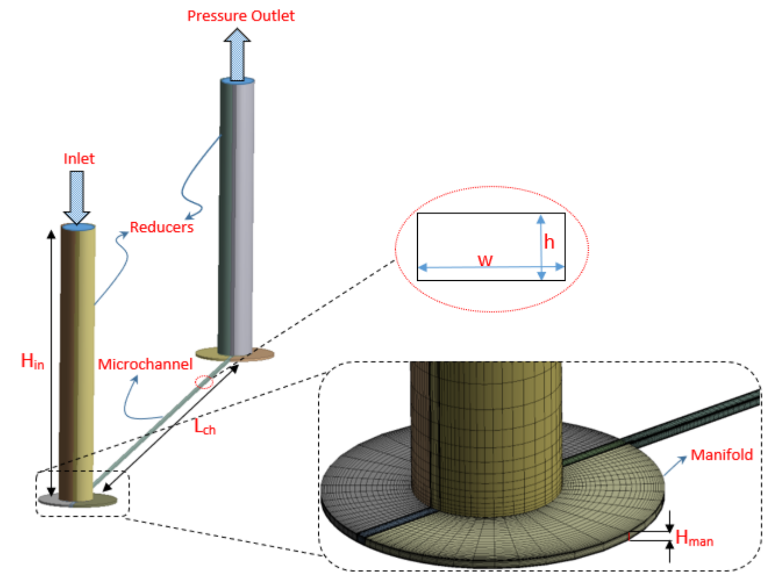

Figure 4: Geometry of the computational domain

for both considered geometries and is vented to the atmosphere using a orthogonal outlet reducer in case of MC and outlet extended domain in MT geometry. The value of turbulence intensity (TI) at the inlet is 5% for all considered Re, the same value adopted by Abraham et al. (2008). However, in current work the inlet boundary condition is set at the entrance of the domain (inlet manifold/reducer) and not at the MC/MT inlet as it was the case with Abraham et al. (2008) and Minkowycz et al. (2009). Hence in laminar regime, due to the fact that reducer section is much longer than manifold, turbulence intensity gets dissipated in the first part of the manifold to a smaller value i.e. close to 1%.

Steady state RANS simulations are performed using the SST k-ω transitional turbulence model. A modified formulation of γ-Re_θ transition turbulence model for internal flows is applied based on the coefficients outlined earlier in Sec. 3. High-resolution turbulence numerics are employed with a higher order advection scheme available in ANSYS-CFX (ANSYS (2018)). Pseudo time marching is done using a redphysical time step of 0.01s. A convergence criteria of 10^{-6} for RMS residuals of governing equations is chosen while monitor points for pressure and velocity at the MC/MT inlet and outlet are also observed during successive iterations. In case where residuals stayed higher than convergence criteria, the solution is deemed converged if monitor points did not show any variation for 200 consecutive iterations. Reference pressure of 101 kPa was used for the simulation and all the other pressures are defined with respect to this reference pressure. Due to small measured surface roughness, walls of the MT/MC are treated as smooth in numerical model. A no slip boundary condition is applied at the walls. Energy equation was activated using the total energy option available in CFX. Kinematic viscosity dependence on the gas temperature is defined using Sutherland's law.

$$\mu = \mu_{ref} \left(\frac{T}{T_{ref}}\right)^{\frac{3}{2}} \left(\frac{T_{ref}+S}{T+S}\right), \tag{20}$$

where constants for Nitrogen gas are:

$$\mu_{ref} = 1.7812 \times 10^{-5}\ Pa\ s$$
$$T_{ref} = 298.15K$$
$$S = 111K$$

Further details of boundary conditions can be seen in Table 4. To estimate

Table 4: Boundary Conditions.

Boundary	**Value**
Inlet	- mass flow rate: experimental or from Eq. 3)
	- Turbulence Intensity, TI = 5%
	- Temperature $T_{in} = 23$ °C
Walls	- No slip
	- Adiabatic
Outlet	Pressure outlet, $p_{out} = p_{atm}$

the average friction factor, two planes defined at x/L of 0.0005 and 0.9995 are treated as the inlet and outlet of MC respectively. Analysis results from these planes are further post-processed in MATLAB to evaluate the numerical friction factors using Eq. 1.

4.4. Grid Independence

Three different meshes were utilized for each cross-section where number of elements are systematically increased as shown in Table 5. The difference between the evaluated friction factor was found to be $\geq 10\%$ from Mesh-A to Mesh-B while it was less than 2% between Mesh-B and Mesh-C. Thus, number of divisions for both cross-sections as shown for Mesh-B in Table 5 are finally utilized. The mesh expansion factor was kept as 1.1 and the first node point was placed such that $y+$, which is the non-dimensional distance between the wall and first node point, was ≤ 1 in the transitional regime and less than 5 for the highest Re simulated. Solution accuracy of Mesh-B for both cross sectional geometries

Table 5: Different meshes used for grid independence study.

Geometry	**A**	**B**	**C**
MT ($r \times L \times \theta$)	20×100×2	40×200×5	40×300×10
MC ($w \times h \times L$)	30×20×100	45×30×200	50×40×300

is demonstrated in Figure 5. An excellent agreement between measured and numerical total pressure drop clearly shows that selected mesh and boundary conditions represent the physics of the problem with sufficient accuracy.

5. Results and Discussion

5.1. Validation

Laminar to turbulent flow transition is established using the average friction factor curve. Re_c is defined as the Reynolds number in correspondence of which the friction factor attains its first minimum and then starts to increase. This point is individuated during MATLAB post processing of experimental and numerical results. Theoretical values of friction factor in the laminar regime for considered test sections can be obtained by the Poiseuille equation for circular tubes and the Shah & London correlation (Shah and London (1978), Sahar et al.

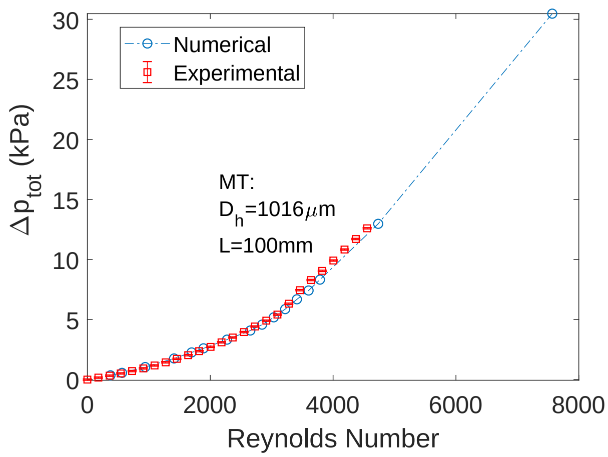

(a)

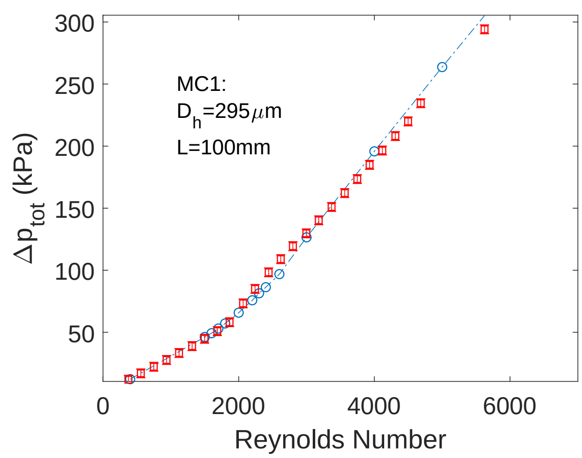

(b)

Figure 5: Comparison of total pressure drop in the assembly for MT (**a**), and MC1 (**b**).

(2017)) for rectangular channels:

$$f_{c,lam} = \frac{64}{Re} \tag{21}$$

$$f_{R,lam} = \frac{96}{Re}\left(1 - 1.3553\alpha + 1.9467\alpha^2 - 1.7012\alpha^3 + 0.9564\alpha^4 - 0.2537\alpha^5\right) \tag{22}$$

For turbulent regime, Blasius law (smooth tubes) can be used to compare the frictional factor results from experimental and numerical analysis of both cross sections:

$$f_B = 0.3164Re^{-0.25} \tag{23}$$

A comparison between numerical and experimental friction factors for circular cross section is made in Figure 6. Numerical results are within the experimental uncertainty in both the laminar and turbulent flow regimes. It can be seen in Figure 6b that the match is excellent in the transitional regime where Re_c is 3100±93 from experimental results and ∼2727 using $\gamma - Re_\theta$ transitional model (-12%). Numerical results in laminar regime are slightly higher than theoretical Poiseuille's law ($f_{c,lam}$) whereas both experimental values and numerical prediction in the turbulent regime are lower than the Blasius law.

A similar comparison between experimental and numerical findings for MC1 is performed in Figure 7. There exists an excellent agreement between the numerical and experimental results in the laminar flow regime where f_f follows the Shah & London correlation ($f_{R,lam}$). In the turbulent flow regime, both experimental and numerical results are slightly above the Blasius law. However, even in the turbulent regime numerical f_f is within the uncertainty of experimental results. It is evident from Figure 7b that the model is able to predict the subtle change in slope of f_f due to the transition from laminar to turbulent flow regime. In fact, the trend of numerical simulation is similar to what is observed in experiments. In transition regime the values of f_f smoothly connect the limiting cases of laminar and turbulent flow regimes. Contrary to what occurs in external flow where there is a sharp transition to turbulence once disturbances break laminar flow stability, in internal flows a region of fully developed intermittent

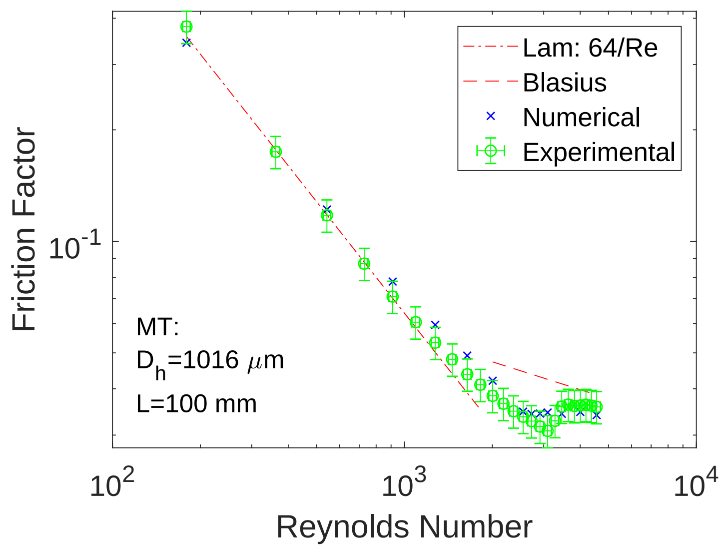

(a)

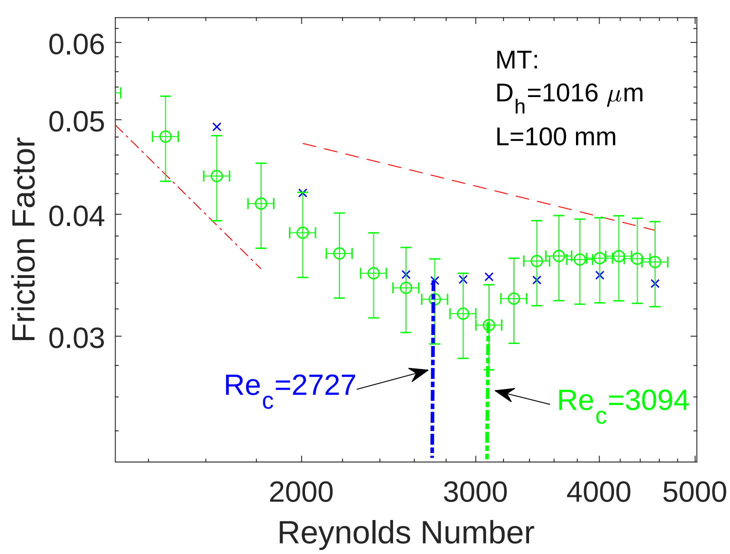

(b)

Figure 6: Friction factor for MT (**a**), and zoomed laminar-to-turbulent transition region (**b**).

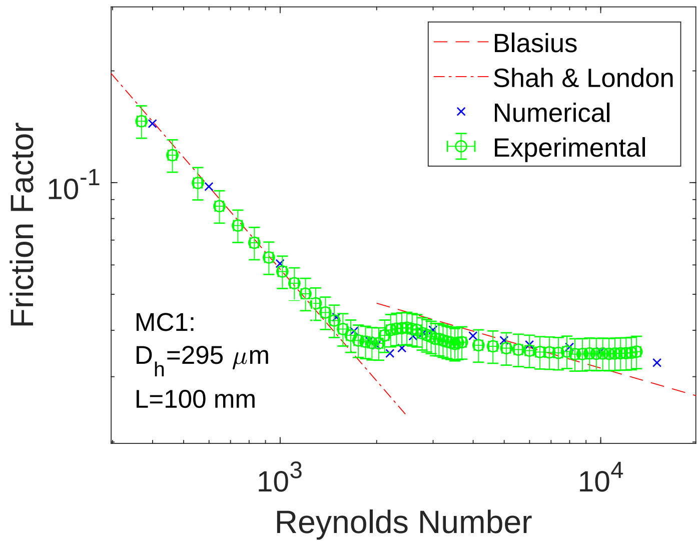

(a)

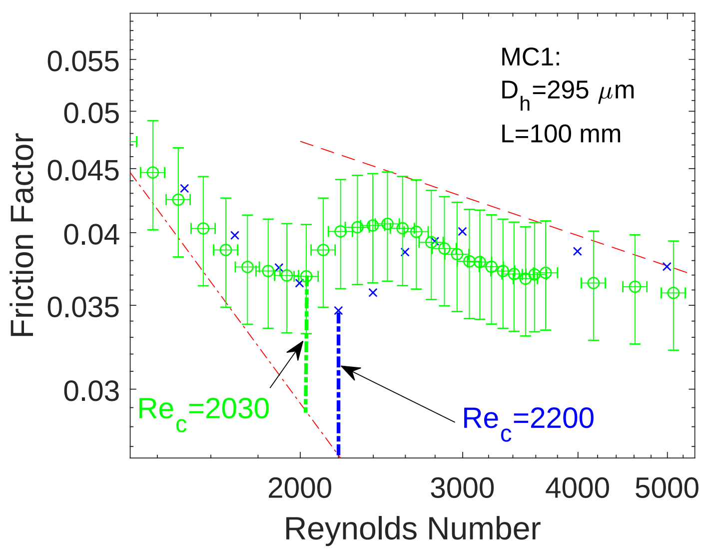

(b)

Figure 7: Friction factor for MC1 (**a**), and zoomed laminar-to-turbulent transition region (**b**).

flow exists (Abraham et al. (2008, 2010)). This interval could be identified in Figure 7a between $Re = 1800$ and $Re = 3000$ for MC1. In this range the agreement between numerical and experimental values is not as good as in the other regimes, but the relative error between the two values remains under 15%. As noted for MT, the intriguing aspect of the $\gamma - Re_\theta$ transition turbulence model is the ability to predict Re_c with sufficient accuracy. In fact, the difference between experimental and numerical Re_c is limited also for MC1. Experiments highlighted a Re_c equal to 2030±61, whereas numerical one is ~ 2200 (+8%). The correct trend is confirmed by MC2 for which f_f is reported in Figure 8. In this case experimental Re_c is observed at 2536±76 whereas model predicts it to be ~ 2800 (+10%). An overview of the main results in terms of comparison between experimental and numerical Re_c is shown in Table 6. Using Menter's $\gamma - Re_\theta$ model as modified by Abraham et al. (2008), the maximum deviation between experimental and numerical values of Re_c is less than 12 % for all the investigated channels. Moreover, Re_c showed a decrease from ~ 2792 to ~ 2200 by increasing the aspect ratio of the rectangular MC (α) from 0.24 to 0.7. This decrease is in agreement with the theoretical trend predicted by Obot-Jones Model (Obot (1988)) developed for macro ducts.

Table 6: Re_c for investigated MT & MCs.

Channel	$\boldsymbol{D_h}$ **($\boldsymbol{\mu}$m)**	$\boldsymbol{\alpha}$	**Exp.** $\boldsymbol{Re_c}$	**Num.** $\boldsymbol{Re_c}$	**Deviation** (%)
MT	1016	1	3094±93	∼2727	11.8
MC1	295	0.7	2030±61	∼2200	8.4
MC2	213	0.24	2536±76	∼2792	10

5.2. Semi-local friction factor

Laminar-to-turbulent flow transition has been studied in the previous section using total pressure loss and therefore average friction factors along the complete length of the MT and MCs were reported. On the other hand, using the Menter's $\gamma - Re_\theta$ turbulence model, the local frictional behavior of the gas flow during

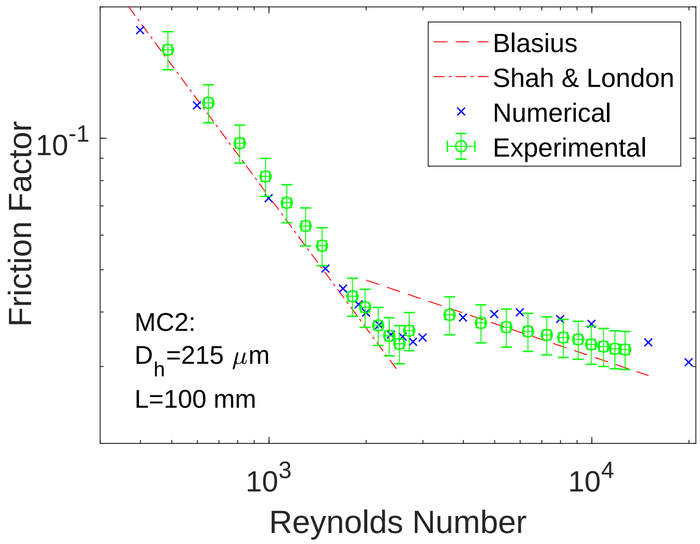

(a)

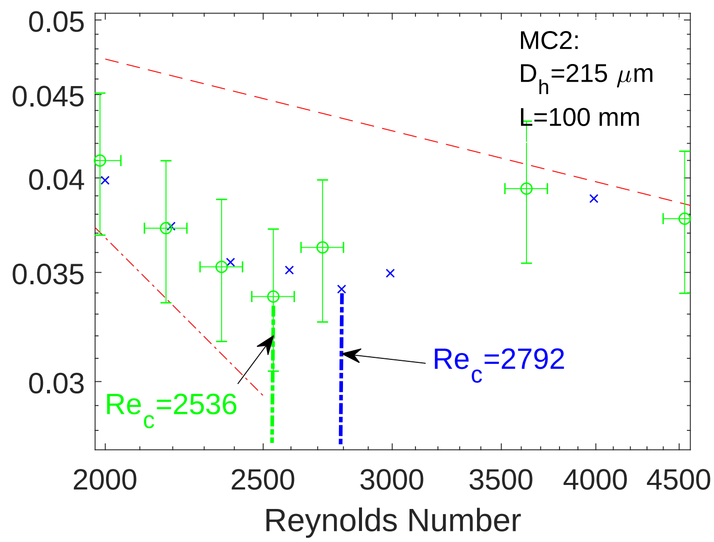

(b)

Figure 8: Friction factor for MC2 (**a**), and zoomed laminar-to-turbulent transition region (**b**).

the transitional flow regime can be elucidated. In the case of MT, a lower f_f has been observed (see Figure 6) in the early turbulent regime when compared to the conventional Blasius law. For microchannels, deviation of the turbulent friction factor (higher or lower than) from Blasius law has also been reported by Morini et al. (2007), Kawashima et al. (2016), Yang et al. (2012), Celata et al. (2009). Since the average value of f_f in microchannels exhibits some deviation from the conventional laws in the turbulent regime, a semi-local analysis of the friction factor values has been performed numerically, by calculating the average value of the friction factor between two fixed axial cross-sections along the channel. Five axial positions along MT have been considered for the semi-local evaluation of the friction factor (x = 0L, 0.25L, 0.5L, 0.75L and L). Semi-local values of f_f between two consecutive sections are evaluated by employing Eq. 1. An additional numerical run for a MT with the same D_h (1016 μm) but an increased length of 400 mm (hereafter referred to as MT-A), is also performed to see any possible effect of the ratio L/D_h on the laminar-to-turbulent transition as well as local turbulent characteristics of the friction factor (determined numerically).

The comparison between the semi-local values and experimental average friction factor values for the two MTs is shown in Figure 9. As expected, semi-local f_f is highest in the upstream part of the MT due to strong inlet effects for both MTs. Strictly speaking, the velocity profile for gas flow inside MT, due to the acceleration caused by the gas compressibility, never reaches a developed profile even if the Mach number in these simulations is always lower than 0.2. Therefore, it is not possible to define hydraulic entry length as in the case of incompressible flows. However, propagating the same idea it is evident that for the MT with smaller L/D_h the developing pressure loss is quite significant and hence causes a higher f_f when x/L is between 0-0.25. The experimental as well as the numerical results of f_f follow the Blasius law in the turbulent flow regime for MT-A (Figure 9b) whereas MT with smaller L/D_h stays 7% lower than the Blasius law at the highest Re simulated (Figure 9a). It is interesting to notice that close to the transitional Re, the semi-local f_f stays consistently lower than the average theoretical values when x/L is between 0.25-0.5 as well

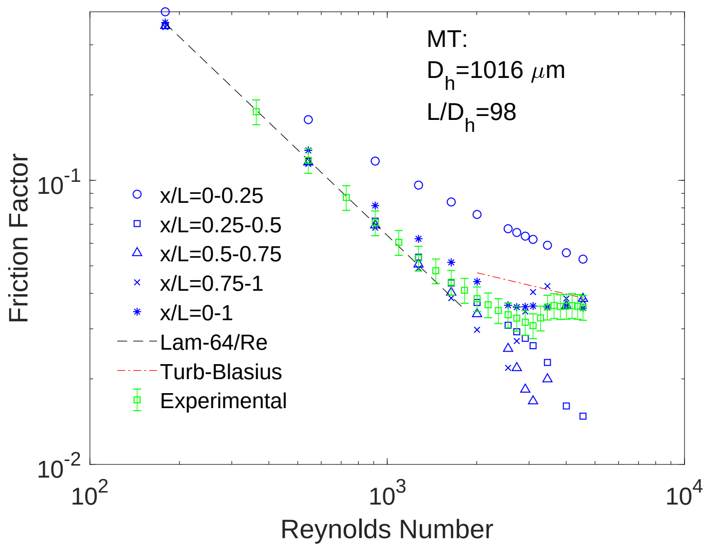

(a)

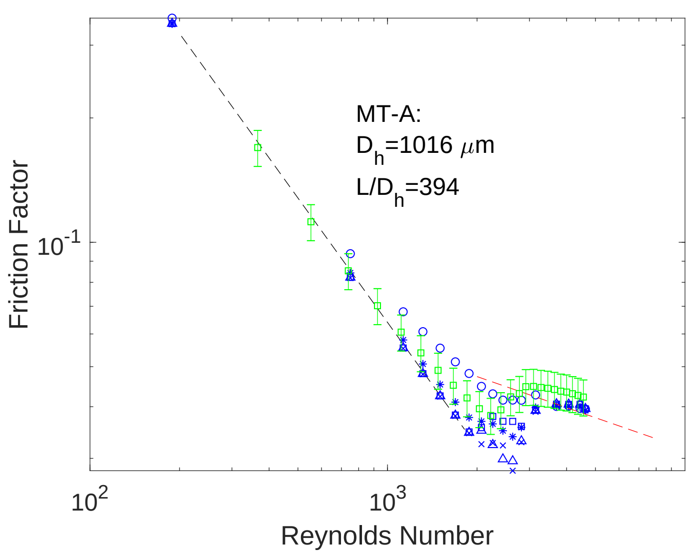

(b)

Figure 9: Semi-local f_f for MT (**a**), and MT-A (**b**).

as 0.5-0.75 whereas it follows the macro laws in the last part of the MT (i.e. x/L between 0.75-1). Therefore, even though in the entrance region, the semi-local f_f is quite high, due to its significant decrease in the transitional regime, the overall average of the evaluated f_f stays slightly lower than the Blasius law. Such lower values of the turbulent frictional factor are also evident in the experimental data of the MT (Figure 9a). On the contrary, such behavior is not observed for the longer tube MT-A and it may be pertinent to MTs having values of $L/D_h \leq$100. Lower values of the local f_f compared to fully developed values are also reported by Abraham et al. (2008) where through the modified Menter's model described before, authors show that an intermittent nature of the flow (neither fully laminar nor fully turbulent) may persist inside the tube which results in a lower value of local f_f compared to the fully developed value (given by Poiseuille's law) between $20 < x/D_h < 115$. Therefore if the length of the tube is considerably short and hydraulic diameter is big enough (100 mm and 1016 μm in the current case, respectively), local f_f may stay lower for most of the length of the MT after an initial hike due to the entrance effects. This ultimately causes the average f_f to be lower than the Blasius prediction in the turbulent regime. However, if L/D_h is reduced further beyond a point, the whole length of the MT is strongly influenced by the entrance effects and the apparent f_f is higher than the conventional laws. This is evident from all the presented results in the range x/L =0-0.25 where the semi-local f_f is much higher than the other semi-local values of the friction factor far from the entrance. Similar findings were reported by Cheng et al. (2017) where they recommended using L/D_h >100 for the evaluation of f_f without significant differences from the conventional theory. Barlak et al. (2011) also found that MTs having a L/D_h smaller than 100, seriously affect the overall f_f due to the entrance effects, by determining higher values of f_f than the Blasius prediction in the turbulent regime. On the other hand, for the tube with L/D_h >100 (MT-A), the semi-local f_f far from the entrance region ($x/L = 0.5 - 0.75$ and $x/L = 0.75 - 1$) follows the conventional laws in the laminar as well as the turbulent regimes by confirming the complete agreement with the conventional theory even for the microchannels. The semi-local values of the f_f shown in Figure 9 demonstrate that the higher values of the f_f close to the entrance region of the channel are the main motivation for the deviation of the average overall friction factor from the Poiseuille's law in the laminar regime when Re increases. On the contrary, the overall friction factor is only marginally higher than the Blasius correlation in the turbulent regime. From the experimental results shown in Figure 9, it can be deducted how MT with $L/D_h \leq 100$ shows a delayed transition compared to the longer MT-A. Re_c decreased from 3094 in the case of $L/D_h = 98$ to 2223 for $L/D_h = 398$. On the contrary, numerical results show that Re_c decreased slightly from ∼2727 to ∼2635 by increasing the L/D_h from 98 to 398. On this point, the comparison between numerical and experimental results is inconclusive and more data needs to be collected to better understand the effect of L/D_h ratio on the critical Reynolds number.

6. Conclusions

In this paper, it has been demonstrated that the laminar-to-turbulent transition for gas microflows can be estimated with acceptable accuracy using Menter's $\gamma - Re_\theta$ transitional turbulence model (Menter et al. (2006)) as modified by Abraham et al. (2008). Validation of the model with experimental results showed that the modified Menter's model predicted the critical Reynolds number linked to the laminar-to-turbulent transition (Re_c) with a maximum error of 11.8% for all the tested channels having different cross-sections and D_h values. Local frictional characteristics showed that for the short MT having $L/D_h \leq 100$, the semi-local f_f are significantly lower than the conventional values for a large part of the MT length, during the transitional and early turbulent regimes. This causes the overall f_f to be lower than the Blasius correlation in the turbulent regime whereas for channels having $L/D_h > 100$, no deviation from the Blasius law is observed.

Credit Author Statement

Danish Rehman: Formal analysis, Investigation, Methodology, Validation, Writing—original draft; Gian Luca Morini: Funding acquisition, Methodology, Supervision, Writing—review & editing

Acknowledgements

This research received funding from the European Union's Framework Programme for Research and Innovation Horizon 2020 (2014–2020) under the Marie Sklodowska-Curie Grant Agreement No. 643095 (MIGRATE Project).

Nomenclature

A	Cross section area of the microchannel/microtube
$c_{\gamma,2}$	Transitional model constant
$c_{\theta,t}$	Transitional model constant
D_h	Hydraulic diameter
E_1, E_2	Intermittency destruction terms
F_1, F_2	Blending functions in SST-k-ω turbulence model
f_f	Fanning friction factor
$f_{c,lam}$	Laminar friction factor for circular cross section
$f_{R,lam}$	Laminar friction factor for rectangular cross section
f_B	Blasius friction factor
$\dot{G}$	Mass flux
h	Height of the microchannel
H_{man}	Height of the manifold
H_{in}	Height of the reducer
k	Turbulent kinetic energy
$\dot{m}$	Mass flow rate
p	Pressure
P_k	Rate of kinetic energy production

$P_{\gamma,1}, P_{\gamma,2}$	Intermittency production terms
$P_{\theta,t}$	Production term for the transition onset Reynolds number
R	Specific gas constant
Re	Reynolds Number
$Re_{\theta,t}$	Transition momentum thickness Reynolds number
S	Absolute value of the shear strain
T	Temperature
u	Velocity of the fluid
w	Width of the microchannel
L	Length of the the microchannel/microtube
$y+$	Non-dimensional distance between the wall and first node element

Greek Symbols

α	Aspect ratio of the microchannel
β_1, β_2	SST model constants
γ	Intermittency factor
ϵ	Surface roughness of the microchannel/microtube
μ	Dynamic viscosity of the fluid
μ_t	Turbulent/eddy viscosity
ν	Kinematic viscosity of the fluid
ρ	Density
τ	Shear stress
χ	SST model constant
ω	Specific rate of turbulent destruction
Ω	Magnitude of the absolute vorticity rate

Subscripts

- $_{av}$ Averaged over the whole length of the microtube/microchannel
- $_{c}$ Critical
- $_{i}$ Cartesian components of the flow quantity
- $_{in}$ at the inlet of the microtube/microchannel
- $_{out}$ at the outlet of the microtube/microchannel
- $_{tot}$ Total (static and dynamic) part of the flow quantity
- $_{w}$ Wall
- $_{x}$ Flow quantity at cross section located at distance 'x' from the inlet

Abbreviations

- 2D/3D Two dimensional and three dimensional
- CFD Computational fluid dynamics
- DNS Direct numerical simulation
- LES Large eddy simulation
- MT Microtube
- MC Microchannel
- PMMA Poly methyl methacrylate (acrylic)
- RANS Reynolds-averaged Navier–Stokes equations
- RMS Root mean squared
- SST Shear Stress Transport
- S&L Shah and London

References

Abraham J, Sparrow E, Tong J. Breakdown of laminar pipe flow into transitional intermittency and subsequent attainment of fully developed intermittent or turbulent flow. Numerical Heat Transfer, Part B: Fundamentals 2008;54(2):103–15.

Abraham J, Sparrow E, Tong J, Bettenhausen D. Internal flows which transist from turbulent through intermittent to laminar. International Journal of

Thermal Sciences 2010;49(2):256–63. doi:10.1016/j.ijthermalsci.2009.07.013.

Adams TM, Dowling MF, Abdelkhalik S, Jeter SM. Applicability of traditional turbulent single-phase forced convection correlations to non-circular microchannels. Int J Heat and Mass Transfer 1999;42(23):4411–5.

ANSYS . Cfx version 18.1 manual. ANSYS, Inc, Cannosburg, PA 2018;.

Asadi M, Xie G, Sunden B. A review of heat transfer and pressure drop characteristics of single and two-phase microchannels. Int J Heat and Mass Transfer 2014;79:34–53.

Avila K, Moxey D, de Lozar A, Avila M, Barkley D, Hof B. The onset of turbulence in pipe flow. Science 2011;333(6039). doi:10.1126/science.1203223.

Barkley D, Song B, Mukund V, Lemoult G, Avila M, Hof B. Eliminating turbulence in spatially intermittent flows. Science 2010;327(5972):1491–4. doi:10.1126/science.1186091.

Barkley D, Song B, Mukund V, Lemoult G, Avila M, Hof B. The rise of fully turbulent flow. Nature 2011;526:550–3. doi:10.1126/science.1203223.

Barlak S, Yapıcı S, Sara O. Experimental investigation of pressure drop and friction factor for water flow in microtubes. International Journal of Thermal Sciences 2011;50(3):361 –8. URL: http://www.sciencedirect.com/science/article/pii/S1290072910002577. doi:https://doi.org/10.1016/j.ijthermalsci.2010.08.018; nano, Micro and Mini Channels.

Celata G, Lorenzini M, Morini G. Friction factor in micropipe gas flow under laminar, transition and turbulent flow regime. Int J Heat Fluid Flow 2009;30:814–22.

Cheng J, Li H, Zhu Z, Tao Z. Numerical simulation of flow transition in a rectangular microchannel. In: ICHMT DIGITAL LIBRARY ONLINE. Begel House Inc.; 2017. p. 1419–28.

Choi S, Barron R, Warrington R. Fluid flow and heat transfer in microtubes. Micromechanical Sensors, Actuators, and Systems, ASME 1991;:123–34.

Dixit T, Ghosh I. Review of micro- and mini-channel heat sinks and heat exchangers for single phase fluids. Renewable and Sustainable Energy Reviews 2015;41:1298–311.

Gorji S, Seddighi M, Ariyaratne C, Vardy A, O'Donoghue T, Pokrajac D, He S. A comparative study of turbulence models in a transient channel flow. Computers Fluids 2014;89:111 –23. URL: http://www.sciencedirect.com/science/article/pii/S0045793013004209. doi:https://doi.org/10.1016/j.compfluid.2013.10.037.

Harms TM, Kazmierczak MJ, Gerner FM. Developing convective heat transfer in deep rectangular microchannels. Int J Heat and Fluid Flow 1999;20(2):149–57.

Hong C, Nakamura T, Asako Y, Ueno I. Semi-local friction factor of turbulent gas flow through rectangular microchannels. International Journal of Heat and Mass Transfer 2016;98:643–9.

Kandlikar SG, Schmitt D, Carrano AL, Taylor JB. Characterization of surface roughness effects on pressure drop in single-phase flow in minichannels. Physics of Fluids 2005;17(100606). doi:https://doi.org/10.1063/1.1896985.

Kawashima D, Asako T. Data reduction of friction factor for compressible flow in micro-channels. International Journal of Heat and Mass Transfer 2014;77:257–61.

Kawashima D, Yamada T, Hong C, Asako Y. Mach number at outlet plane of a straight micro-tube. Proceedings of the Institution of Mechanical Engineers, Part C: Journal of Mechanical Engineering Science 2016;230(19):3420–30. URL: https://doi.org/10.1177/0954406215614598. doi:10.1177/0954406215614598. arXiv:https://doi.org/10.1177/0954406215614598.

Kühnen J, Song B, Scarselli D, Budanur NB, Riedl M, Willis AP, Hof MAB. Destabilizing turbulence in pipe flow. Nature Physics 2018;14.

Kim B. An experimental study on fully developed laminar flow and heat transfer in rectangular microchannels. International Journal of Heat and Fluid Flow 2016;62:224–32.

Launder B, Spalding D. The numerical computation of turbulent flows. Computer Methods in Applied Mechanics and Engineering 1974;3(2):269 –89. URL: http://www.sciencedirect.com/science/article/pii/0045782574900292. doi:https://doi.org/10.1016/0045-7825(74)90029-2.

Li H, Olsen MG. Aspect ratio effects on turbulent and transitional flow in rectangular microchannels as measured with micropiv. Journal of fluids engineering 2006;128(2):305–15.

Menter F, Langtry R. Transition modelling for turbomachinery flows. In: Low Reynolds Number Aerodynamics and Transition. InTech; 2012. .

Menter FR. Two-equation eddy-viscosity turbulence models for engineering applications. AIAA journal 1994;32(8):1598–605.

Menter FR, Langtry RB, Likki S, Suzen Y, Huang P, Völker S. A correlation-based transition model using local variables—part i: model formulation. Journal of turbomachinery 2006;128(3):413–22.

Minkowycz W, Abraham J, Sparrow E. Numerical simulation of laminar breakdown and subsequent intermittent and turbulent flow in parallel-plate channels: Effects of inlet velocity profile and turbulence intensity. International Journal of Heat and Mass Transfer 2009;52(17-18):4040–6.

Morini G. Laminar to turbulent flow transition in microchannels. Microscale Thermophysical Eng 2004a;8:15–30.

Morini G, Lorenzini M, Salvigni S, Spiga M. Analysis of laminar-to-turbulent transition for isothermal gas flows in microchannels. Microfluidics and Nanofluidics 2009;7(2):181–90.

Morini GL. Single-phase convective heat transfer in microchannels: a review of experimental results. International journal of thermal sciences 2004b;43(7):631–51.

Morini GL, Lorenzini M, Colin S, Geoffroy S. Experimental analysis of pressure drop and laminar to turbulent transition for gas flows in smooth microtubes. Heat Transfer Engineering 2007;28(8-9):670–9. doi:10.1080/01457630701326308.

Obot N. Determination of incompressible flow friction in smooth circular and noncircular passages: A generalized approach including validation of the nearly century old hydraulic diameter concept. J Fluids Eng 1988;110:431–40. doi:https://doi.org/10.1115/1.3243574.

Peiyi W, Little W. Measurement of friction factors for the flow of gases in very fine channels used for microminiature joule-thomson refrigerators. Cryogenics 1983;23(5):273 –7. URL: http://www.sciencedirect.com/science/article/pii/0011227583901509. doi:https://doi.org/10.1016/0011-2275(83)90150-9.

Peng X, Peterson G, Wang B. Frictional flow characteristics of water flowing through rectangular microchannels. Experimental Heat Transfer An International Journal 1994;7(4):249–64.

Rehman D, Morini GL, Hong C. A comparison of data reduction methods for average friction factor calculation of adiabatic gas flows in microchannels. Micromachines 2019;10(3):171.

Reynolds O. Xxix. an experimental investigation of the circumstances which determine whether the motion of water shall be direct or sinuous, and of the law of resistance in parallel channels. Phil Trans R Soc 1883;174. doi:https://doi.org/10.1098/rstl.1883.0029.

Sahar AM, Wissink J, Mahmoud MM, Karayiannis TG, Ishak MSA. Effect of hydraulic diameter and aspect ratio on single phase flow and heat transfer in a rectangular microchannel. Applied Thermal Engineering 2017;115:793–814.

Shah R, London A. Laminar Flow Forced Convection in Ducts. Academic Press, 1978. URL: http://www.sciencedirect.com/science/article/pii/B9780120200511500061. doi:https://doi.org/10.1016/B978-0-12-020051-1.50006-1.

Tuckerman D, Pease R. High-performance heat sinking for vlsi. IEEE Electron Device Lett 1981;5:126–9. doi:doi:10.1109/EDL.1981.25367.

Wibel W, Ehrhard P. Experiments on the laminar/turbulent transition of liquid flows in rectangular microchannels. Heat Transfer Engineering 2009;30(1-2):1298–311. doi:https://doi.org/10.1080/01457630802293449.

Wilcox DC. Re-assessment of the scale-determining equation for advanced turbulence models. AIAA journal 1988;26(11):1299–310.

Wilcox DC. Formulation of the k-w turbulence model revisited. AIAA journal 2008;46(11):2823–38.

Wu X, Moin P, Adrian RJ, , Baltzer JR. Osborne reynolds pipe flow: Direct simulation from laminar through gradual transition to fully developed turbulence. PNAS 2015;112(26):7920–4. doi:https://doi.org/10.1073/pnas.1509451112.

Yang Y. Experimental and Numerical Analysis of Gas Forced Convection through Microtubes and Micro Heat Exchangers. PhD dissertation, Alma Mater Studiorum- Universita di Bologna, 2012.

Yang Y, Brandner J, Morini G. Hydraulic and thermal design of a gas microchannel heat exchanger. Journal of Physics: Conference Series 2012;362. doi:10.1088/1742-6596/362/1/012023.